ELSEVIER

Contents lists available at ScienceDirect

Results in Physics

journal homepage: www.elsevier.com/locate/rinp





Evolutions of morphology and electronic properties of few-layered MoS₂ exposed to UVO

Jinxin Liu ^a, Kuanglv Sun ^a, Xiaoming Zheng ^{a, b}, Shitan Wang ^a, Shichang Lian ^a, Chuyun Deng ^c, Haipeng Xie ^a, Xueao Zhang ^b, Yongli Gao ^d, Fei Song ^e, Han Huang ^{a, *}

- a Hunan Key Laboratory of Super-microstructure and Ultrafast Process, School of Physics and Electronics, Central South University, Changsha 410083, PR China
- ^b College of Physical Science and Technology, Xiamen University, Xiamen 361005, China
- ^c College of Arts and Science, National University of Defense Technology, Changsha, Hunan 410073, China
- ^d Department of Physics and Astronomy, University of Rochester, Rochester, NY 14627, USA
- ^e Shanghai Synchrotron Radiation Facility, Shanghai Institute of Applied Physics, Chinese Academy of Sciences, 239 Zhangheng Road, Pudong New Area, Shanghai 201204, PR China

ARTICLE INFO

Keywords: MoS₂ Ultraviolet ozone Inhomogeneous oxidation Photoelectron spectroscopy Raman and PL spectroscopy

ABSTRACT

Ultraviolet-Ozone (UVO) treatment has potentially promoted the long-term stability and the high performance of two-dimensional-material-based devices. However, the detailed evolutions of materials upon UVO treatment are less reported and unclear. Herein, we have systematically investigated the evolutions of morphology and electronic properties of the UVO treated few-layered MoS₂. A weak p-doping effect on a 1-hour-UVO-exposed bulk MoS₂ is revealed by photoelectron spectroscopy, being attributed to the charge transfer from MoS₂ to the newlyformed MoO_x. Optical microscopy, atomic force microscopy, Raman and PL mapping measurements reveal an inhomogeneous change of MoS₂ morphology after UVO treatment. The oxidation is initiated at intrinsic defect sites and dislocations, and then expands in-plane from dislocations to both sides to form one dimensional standing-wave-like features. The dangling-bond-free surface regions remain smooth, being attributed to the higher energetic barrier for O_2 dissociation and chemisorption. A model is proposed to explain the mechanism of inhomogeneous oxidation. The rather different oxidation behavior of MoS₂ compared with MoSe₂ and MoTe₂ can be attributed to the difference in the in-plane chemical bonds. Our findings remind that the device design with UVO oxidation need to take the microstructure changes after treatment into account instead of only taking notice of the doping effect for performance improvement.

Introduction

Two-dimensional (2D) materials, especially transition metal dichal-cogenides (TMDCs), have expanded rapidly for the platform of low-dimensional physics and various applications [1–3]. Despite broad prospects, lots of 2D materials suffer poor stability under ambient environments compared to their 3D counterparts, since they are highly prone to chemical degradation [4]. In a few hours, BP and metallic TMDCs (e.g., 1T-TiSe₂) exhibit noticeable changes in surface morphology [5,6]. Besides, mechanically exfoliated monolayer high-temperature superconductor $\rm Bi_2Sr_2CaCu_2O_{8+\delta}$ degenerated soon to be insulating due to water vapor induced corrosion and rapid oxygen dopant loss [7]. Worse still, illumination in minutes under ambient conditions results in few-layered ferromagnetic semiconductor CrI₃

flakes into liquid [8]. Natural oxidation of 2D materials has adverse effects on their performance and hampers investigating their intrinsic properties [9].

Several methods have been employed to improve the air stability, such as surface encapsulation, avoidance of light and surface dense oxides [9–13]. Surface encapsulation using h-BN or ALD-Al $_2$ O $_3$ can alleviate degeneration as well as improve device interface quality and carrier mobility [10,14,15]. However, large-cost and time-consuming are required. Very recently, a photoinduced oxidation process of monolayer WS $_2$ in ambient has been reported [12]. Avoidance of light illumination is required for some easily oxidated 2D materials.

Controlled surface oxidation has earned attention via exposing 2D materials to oxygen atmosphere [16–18]. Upon exposure in air, spontaneous oxidation of InSe takes place and the inner layer can be oxidized

E-mail address: physhh@csu.edu.cn (H. Huang).

^{*} Corresponding author.

owing to the loose surface oxides [16]. A dense $\rm In_2O_3$ capping layer can be formed on top of few-layered InSe flakes via a dry-oxidation process. The corresponding FETs show a high mobility of 423 cm²/V·s and an enhanced device lifetime over one month in environment, being attributed to the effective unpinning of the Fermi level at the interfaces of metal-semiconductor contacts and the passivation of capping layer [16]. For exposure to oxygen atmosphere, in spite of the enhanced performance, the doping is unstable and uncontrollable owing to the weak adsorption of newly formed oxides to 2D materials. Although oxygen plasma treatment can result in oxide layers rapidly, the induced possible structural defects and uncontrollability hamper the application in TMDCs [18].

In recent years, Ultraviolet-ozone (UVO) treatment has been demonstrated as an efficient, controllable, and common surface oxidation means for enhancing the stability and performance of TMDCs [19-23]. As we previously reported, UVO treatment causes the formation of uniform and dense oxide layer with high work function in a layerby-layer mode on top of MoSe₂ (MoTe₂) [19-21], which can hinder further oxidation and improve the air stability and can lead to p-doping via surface charge transfer method to build p-n MoSe₂ homojunctions with high photovoltaic performance [20] as well as to a huge improvement in electrical performance of MoTe₂ by lowering Schottky barriers [21]. MoS₂, one of the most extensively studied TMDCs, is less susceptible to oxidation compared with MoSe2 and MoTe2. The theoretical calculations show that the barrier of O2 dissociation at the MoS2 edge is 0.31 eV and that at the basal plane is 1.6 eV, interpreting that O2 can easily decompose into O atoms at the MoS₂ edge but not on the MoS₂ basal plane [24]. However, the oxidation barrier is reduced to 0.8 eV when S vacancy exists on the MoS₂ basal plane, which makes oxidation easy [24]. Therefore, in experiments, it is possible to have different oxidation behaviors at the basal plane, S vacancies and edges of MoS₂, which may be different to MoSe2 and MoTe2. The possible difference of UVO on MoS2 calls for more experimental investigations.

In this letter, mechanically-exfoliated few-layered MoS2 flakes with different UVO treated duration have been systematically investigated via Optical microscopy (OM), atomic force microscopy (AFM), Raman and PL spectroscopy. A weak p-doping effect is observed on a 1-hour-UVO-exposed bulk MoS2 via X-ray/ultraviolet photoemission spectroscopy (XPS, UPS) measurements, and attributed to the charge transfer from MoS2 to the newly-formed MoOx. Raman, PL and AFM measurements demonstrate an inhomogeneous morphology change, indicating that the oxidation is initiated at intrinsic defect sites and dislocations, and then expanded in-plane from dislocations to both sides to form one dimensional standing-wave-like features. The dangling-bond-free surface regions remain smooth due to the higher surface activation energy for O2 dissociation. The difference in the in-plane chemical bonds compared to MoSe₂ and MoTe₂ is the main reason for the rather different UVO oxidation process of MoS2. Our findings indicate that the device design with UVO oxidation can not only take notice of the doping effect, but also need to take the microstructure changes after treatment into account.

Experimental setup and sample characterization

The bulk MoS_2 crystals were purchased from Shanghai Onway Technology Co., Ltd. The MoS_2 flakes were mechanically exfoliated onto 300 nm SiO_2/Si substrates, and then exposed to UVO with the power density of 14.76 mW/cm2 (one centimeter distance from the UV lamp) generated via commercial equipment (Bioforce UV/Ozone Procleaner TM Plus) [21].

Raman and PL measurements were performed on a confocal micro-Raman spectroscope (Renishaw inVia Qontor, UK) with a solid-state laser at 532 nm. The Raman signals were collected through a 100x objective (NA = 0.85) and dispersed by a grating of 1800 lines/mm ensuring a high spectral resolution of $\sim\!1.0~{\rm cm}^{-1}$ and a fitted peak position accuracy of 0.1 cm $^{-1}$. The Raman and PL mapping were measured

at a high confocal mode with a \sim 0.8 um laser spot size and 0.5 um step [25]. For PL measurements, a grating of 600 lines/mm was used. The laser power was set well below 0.1 mW to avert any destructions to MoS₂. The morphologies of the flakes were monitored by OM (Leica DM2500, Germany) and AFM (Agilent 5500, US) in a tapping mode [26]. The thickness was firstly identified via optical method and further verified by high confocal Raman method. UPS and XPS characterizations were carried out in a SPECS system [27]. All the measurements were performed at room temperature.

Results and discussions

Due to the limitation of the large light spot in milimeter scale, a bulk MoS₂ sample is used for photoemission spectroscopy measurements. To study the evolutions of MoS₂ surface electronic states and compositions upon UVO exposure, XPS measurements were carried out. The Mo 3d, O 1s and S 2p core level spectra of pristine and 1-hour-UVO-treated MoS2 are shown in Fig. 1a, b and c. For pristine sample, the Mo 3d spectrum consists of three peaks located at around 227.4, 230.1 and 233.3 eV, corresponding to S 2s (orange), and spin-orbital interaction induced $Mo^{4+} 3d_{5/2}$ and $3d_{3/2}$ (blue) doublet of pristing MoS_2 [28], respectively. For exposed sample, extra doublet peaks (green) located at 232.8 and 236.0 eV are correspond to Mo^{6+} $3d_{5/2}$ and $3d_{3/2}$ components of nonstoichiometric molybdenum oxide (MoO_x with x < 3). Fig. 1b also suggests that the oxidation product is MoO_x. Similarly, in the S 2p spectra, except for the doublet peaks of pristine MoS2, additional doublet peaks appear at 165.1 and 166.3 eV arising from S-O bonding [29]. Peak broadening is evident after UVO treatment, indicating the change of surface chemical order. Substoichiometric MoS_{2-x} caused the S 2p doublet characteristic broadening, indicating the removal of sulfur atoms from the surface [30]. MoS₂ related Mo 3d and S 2p doublet peaks are slightly downshifted by ~0.27 eV after UVO treatment, indicating the downshift of Femi level toward the VBM, confirming that the ndoping level of MoS₂ is weakened. The smaller intensity ratio $I_{Mo^{6+}}/I_{Mo^{4+}}$ confirms that the oxidation process is self-limited at topmost several layers or inhomogeneous.

Fig. 1d and e show the corresponding UPS results. The valence band (VB) edge of the pristine bulk MoS2 (the black plot in Fig. 1d) is 1.18 eV below the fermi level. Considering the band gap of \sim 1.29 eV [31], bulk MoS₂ is n-type. The secondary electron cutoff in Fig. 1e shows the work function (WF) of bulk MoS2 measured to be 4.65 eV. These results are in good agreement with previous literatures [32]. Upon exposure, the MoS₂ related features disappeared and a new VB edge emerged at 3.18 eV (Fig. 1d, red), which is comparable to the band gap of 3.27 eV for MoO₃ [33], also suggesting the formation of MoO_x on MoS₂. However, the WF only increases by 0.43 eV to 5.08 eV, smaller than that (6.8 eV) for MoO₃ [33], which indicates that the oxide layer is inhomogeneous or quite thin via a self-limited oxidation process at topmost several layers. Owing to the higher WF of the newly formed MoO_x [34], charge transfer from MoS₂ to it is expected. Fig. 1f shows the band diagrams at MoO_x /MoS₂. Except for the 0.27 eV upward band bending, a surface dipole of 0.16 eV pointing to the surface is formed at the interface. We have previously reported that for both bulk MoTe2 and MoSe2 treated using the same method but for less duration the band can upshift by up to \sim 0.75 eV [20,21]. To reveal the possible underlying mechanism, we have systematically explored the physical effects of UVO exposure on mechanically exfoliated few layered MoS2 flakes at nanometer scale.

Fig. 2a shows an optical image of the as-exfoliated MoS_2 flake consist of single layer (1L), bilayer (2L), and trilayer (3L) with different contrast. Corresponding AFM image in the black solid square in Fig. 2b shows a smooth surface with a root-mean-square (RMS) of 0.2 nm. The inserted line profile reveals a ~ 1.0 nm step height, higher than that of 1L MoS_2 [35], which may be attributed to the effect between tip and samples. Fig. 2c shows the typical Raman spectra of 1–3 L MoS_2 , respectively. Two characteristic Raman peaks can be observed in 1L

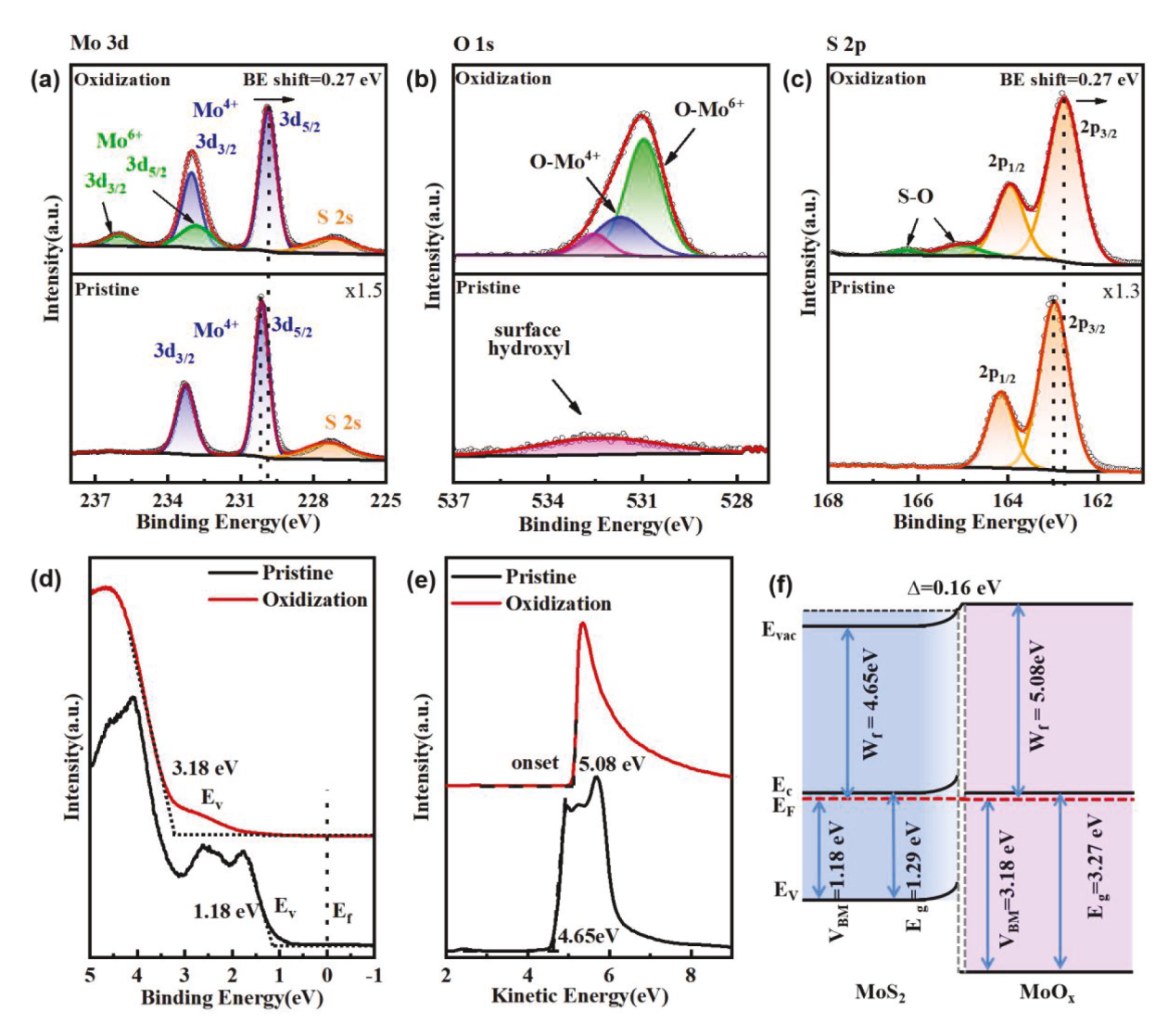


Fig. 1. XPS and UPS characterizations of bulk MoS₂ before and after exposing to UVO for 1 hr: Mo 3 d (a), O 1s (b) and S 2p (c) core level spectra. White dots are experimental data. Blue, green and orange curves are the corresponding fitting curves, respectively. Valence (d) and secondary electron cutoff (e) regions of UPS spectra. (f) The band diagrams of MoS₂ after treatment. (For interpretation of the references to colour in this figure legend, the reader is referred to the web version of this article.)

 MoS_2 located at 384.9 ($E_{2\alpha}^1$) and 404.2 cm⁻¹ (A_{1g}), respectively. The insert in Fig. 2c shows the A_{1g} , E_{2g}^1 phonon modes shift oppositely and their frequency difference increases with the number of layers as 19.3, 21.8, and 23.6 cm⁻¹ for 1L-, 2L-,3L-MoS₂ respectively. Such trend can be attributed to the interlayer vdW interactions and the corresponding dielectric screening [36–39]. Due to the transition from indirect to direct gap with the thickness decreasing from bulk to monolayer [31], PL is a facile method to judge the number of layers of TMDCs. Fig. 2d displays the PL spectra of 1L- to 3L-MoS $_2$, respectively. There are two prominent peaks at \sim 1.85 (A) and \sim 2.05 eV (B) from the direct gap transition at K (K') point [31,40], and their energy difference is the spin-orbital interaction induced valence-band splitting. Peak A becomes stronger as the number of layers decreasing. The weak PL peak (I) related to the indirect band gap transition is detected for 3L- and 2L-MoS2 but not for 1L-MoS2 [31]. All the results in Fig. 2 reveal the high quality of our mechanically exfoliated samples.

The morphology and corresponding optical properties of above MoS₂ flakes upon 6 min UVO exposure were characterized using OM, AFM, Raman and PL spectroscopy, respectively. Compared to pristine sample (Fig. 2a), the 1L regions disappeared (Fig. 3a). AFM image in Fig. 3b from the white square in Fig. 3a shows obvious morphology changes.

Especially for 1L MoS $_2$, it became rougher with discontinuous protrusions. The insert in Fig. 3b shows a close-up AFM image. The corresponding Raman and PL spectra show no MoS $_2$ related peaks (Fig. S1a and b). Moreover, no MoO $_3$ related peak can be observed. Thus, 1L MoS $_2$ has been entirely oxidized into Raman-inactive MoO $_x$, consistent with above XPS results.

In thicker regions (>2 layers), rather than homogeneous oxidation as on MoSe2 and MoTe2 [19,20], the oxidation takes place inhomogeneously, as shown in Fig. 3c and d. This inhomogenoeous oxidation is widely observed in MoS2 as shown in Fig. S2. Triangular etching pits [41] were observed neither in single-layer nor multilayer MoS₂ samples. This can be attributed to that the produced MoO_x could not volatize at ambient conditions and agglomerate together to form larger 3D clusters on the base plane of MoS2 in various sizes around step edges and dislocations, due to the dangling-bond-free surface of MoS2 with higher activation energy [42]. Oxidation occurs more intensively where the clusters are larger, as evidenced by Raman and PL results shown in Fig. S1c and d. The Raman (PL) intensity in large cluster regions (red square region in Fig. 3c) is weaker (much stronger) than in small cluster regions (blue triangle region in Fig. 3c), indicating that the large cluster regions have been fully thinned into 1L MoS2 while the smaller cluster regions remain at least 2L MoS₂. The redshift of Raman peak A_{1g} (2.7

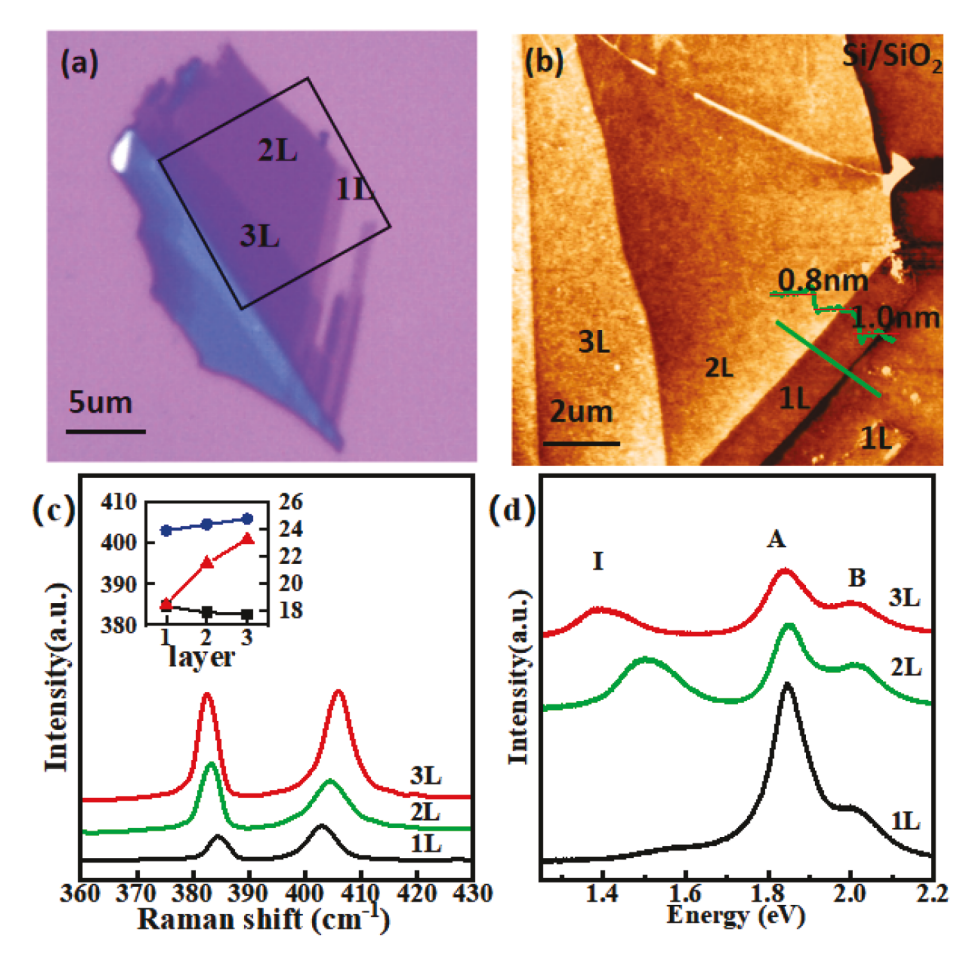


Fig. 2. Characterizations of mechanically-exfoliated MoS₂ on SiO₂/Si. (a) Optical image of the as-prepared MoS₂ flake containing various number of layers. (b) Corresponding AFM image in the black solid square in (a). Raman (c) and Photoluminescence (d) spectra of as-prepared 1–3 layered MoS₂ at room temperature. The insert in (c) shows variation of the A_{1g} , E_{2g}^{1} phonon modes and their frequency difference with the number of layers.

 ${\rm cm^{-1}}$ for large cluster regions VS 0.2 ${\rm cm^{-1}}$ for small cluster regions) indicates the P doping in MoS₂ flakes, consistent with above XPS results.

It is well known that the TMDC surface is more reactive along with the chalcogen varies from S to Se and then to Te. While the atomic radius increases as X changing from S to Te, the interaction between sp orbital of X and the d band of Mo becomes weaker. According to a RMS roughness research, the values of MoS_2 are relatively low (\sim 0.2–0.4 nm) and almost constant over 27 days; $MoSe_2$ had a value of 27 nm after 9 days of preparation; surface features of $MoTe_2$ were undetectable after 3 days [43]. The order of instability can be largely attributed to the electronegativity of the nonmetallic elements. The larger the electronegativity of the X atom, the more electrons are transferred from M to X; and stronger M—X bonds are formed [44]. The different UVO oxidation process of MoS_2 with that of $MoSe_2$ and $MoTe_2$ can be attributed to the difference in the in-plane chemical bonds.

Fig. 4a shows a series of UVO exposure time dependent OM images (0, 8, 16, 24 min) of a large scale 3L MoS $_2$ flake to display the morphology evolution with exposure time. Fig. S3 shows more details at fewer intervals. The darker the contrast is, the thicker the MoS $_2$. The pristine 3L MoS $_2$ flake appears uniform. Upon 8 min UVO exposure, some cracks (lighter lines) appear, attributed to the oxidation induced thinning as for 2L MoS $_2$. Previous results of oxidative etching on MoS $_2$ reveal that oxidative etching starts at edges, grain boundaries and intrinsic atomic defects where unsaturated S atoms are abundant. The etching prefers to propagate along the crystallographic directions of $< 10\overline{10} >$ with weak bond strengths and generated extra zigzag Mo edges in the domains [45,46]. We attributed the formation of the cracks here to the same mechanism. Such cracks connected to each other and

became wider as exposure time increase to 16 and 24 min while the density had no obvious change, confirming the oxidation initiated along dislocations whose number is a constant for a given flake and expanded in-plane to both sides.

The AFM image in Fig. 4b clear displays the final morphology and further confirms above discussion. The corresponding OM image is inserted. Similar to Fig. 3c, three typical features can be observed. Large but scattered 3D clusters with an averaged diameter of 330 \pm 50 nm and a height of 25 \pm 5 nm in the cracks are labeled as region C. Small but dense protrusions in parallel lines spaced 145 \pm 45 nm on the both sides of cracks and inner sides of step edges or concentric circles on the basal plane with a major height of 6 ± 4 or 14 ± 4 nm are labeled as region B, as evidenced by the zoomed-in AFM image in Fig. S4 and by the statistic results in Fig. S5. It is reported that a linear defect in 2D materials will generated a series of parallel wavelike ripples. In suspended pristine MoS₂, a quasi-periodic structure with all ripples nearly parallel to each other and with height variations up to tens of nanometers has been reported [47]. The parallel ripples bring about a periodic compressive field and considerably reduce the activation energy of the monovacancies diffusion. Recently, in-situ ADF-STEM results suggest that S vacancies tend to migrate to the tip of linear defect rather than the side to elongate the linear defect, which also results in the formation of 2D voids and attached Mo clusters [48]. The linear features in regions B were proposed to arise from such ripples in MoS₂, although a direct evidence is absent. Such ripples also give rise to the intercalation of O₂ in between MoS2 layers. The inner regions surrounded by regions B with smoothest surfaces are labeled as regions A, which are inert to UVO and appear almost as before in both OM and AFM images.

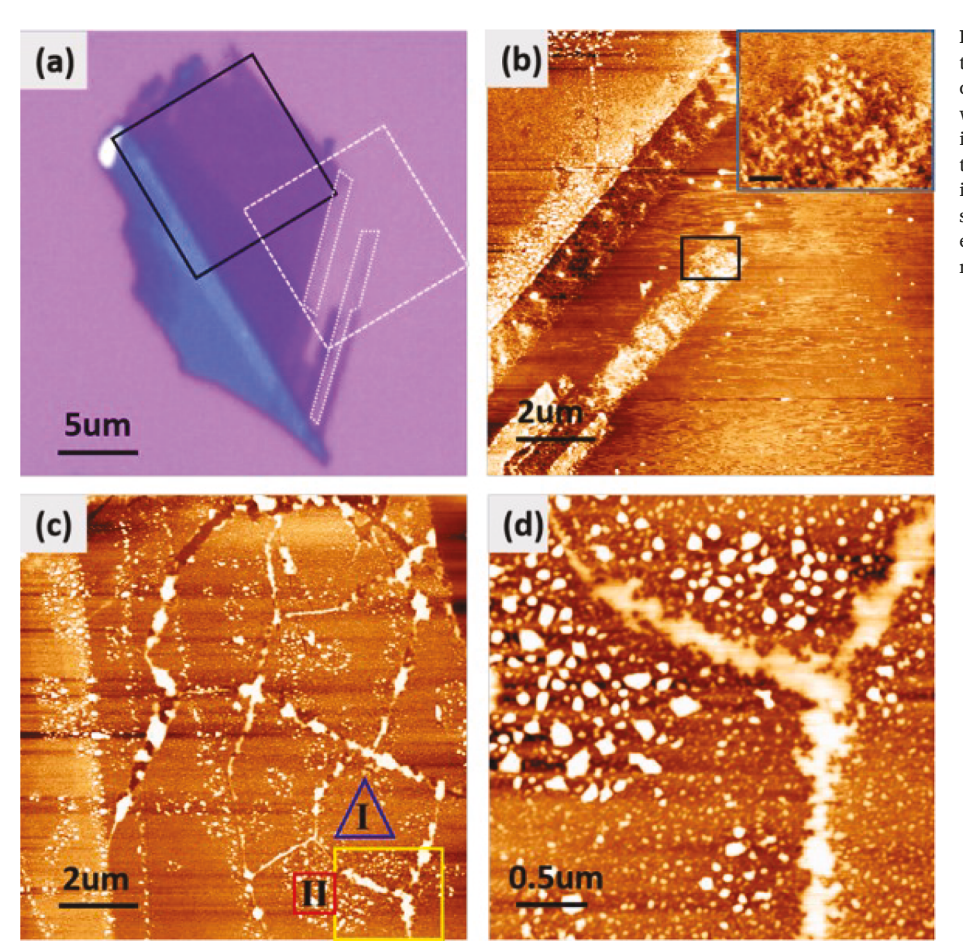


Fig. 3. Different layers (1–3) MoS₂ upon 6 min treatment. (a) Optical image showing vanished contrast in monolayer regions. (b) AFM image in the white dash square in (a). Insert: a close-up AFM image with the scale bar of 200 nm. (c) AFM image in the black solid square in (a). (d) Zoomed-in AFM image around the grain boundary from the yellow solid square in (c). (For interpretation of the references to colour in this figure legend, the reader is referred to the web version of this article.)

Fig. 4c and d present PL and Raman (A1g peak) intensity maps from the white solid square in Fig. 4a, respectively. A zoomed-in AFM image is overlapped on panel d with 65% transparency. At a glance, regions A have weaker PL emission but stronger Raman intensities thanks to the multilayer nature and corresponding in-direct band gap. Although the zoomed-in AFM image in Fig. S4a shows weak contrast in regions A, the crystal lattice keeps intact. On the contrary, Regions C have much stronger PL emission but weaker Raman intensities, indicating single layer nature due to oxidation induced thinning effects and corresponding indirect to direct band gap transition. Several regions (D) in regions C with almost disappeared PL emission and Raman signals can be attributed to the degraded 1L MoS2, where direct excitonic recombination is inhibited by the defect-induced midgap states [49]. This suggests that the newly formed oxides layer delay the oxidation speed in the outof-plane direction. The detailed distribution of such four regions is highlighted in the same PL intensity map in Fig. S6.

Interestingly, the strongest PL emission is observed in regions B, where the Raman intensity are stronger than regions C but weaker than regions A. To understand such a phenomenon, typical PL and Raman spectra from regions A, B, C, D are plotted in Fig. 4e and f. In regions D, both Raman and PL intensities are much weaker than the others. In regions A, the Raman intensity is strongest and the Raman peak difference is $23.4~\text{cm}^{-1}$, confirming the 3L nature. Consistently, PL spectrum in regions A shows an indirect transition, as shown in Fig. S7a. The intensity of PL peak A is slightly enhanced relative to the pristine 3L MoS₂, attributed to the physical adsorption of O₂ on MoS₂ base plane [50]. In regions B and C, the Raman peak differences are both ~21.1 cm⁻¹, close to that of modified 1L MoS₂ [46,51], indicating higher S vacancy density than as-exfoliated samples. This implies that the UVO starts interacting with buried MoS₂ layers and takes off some S atoms. However, the

Raman intensity in regions B is about twice of that in regions C, indicating more 1L MoS $_2$ illuminated by the laser. Given the laser spot size a constant, the most likely reason is that electronically coupled bilayer becomes to two decoupled 1L MoS $_2$ due to the UVO-induced insertion of oxygen [28,52]. One other possible reason is that due to the electron transfers from underlying MoS $_2$ to newly formed MoO $_x$ layers, an effective electric field perpendicular to the base plane of MoS $_2$ is built. Such an external electric field can turn electronically coupled bilayer to decoupled [53]. Such decoupling will result in indirect-to-direct band gap transition and PL enhancement, contributing the strongest PL emission in regions B.

The asymmetric PL peak broadening in regions C can be related to the existence of extra defects induced phonons deriving from oxide centers in UVO-treated MoS $_2$ [54]. Thus, PL emission intensity in regions C is not as strong as as-exfoliated 1L MoS $_2$. The PL peak A blueshift of ~25 meV in regions C relative to that in regions B could be associated with UVO-induced p-type doping [22], consistent with the Raman peak A $_{1g}$ blueshift in Fig. S7b. For the same reason, a slight blueshift and a lower ratio of X/X is observed in regions B compared to pristine monolayer MoS $_2$ [55], shown by the corresponding deconvoluted PL spectra in Fig. S7c.

To intuitively depict the inhomogeneous oxidative process, a carton in Fig. 5 is proposed. The oxidation is initiated at the grainboundaries along $<\!10\overline{10}>$ direction of MoS $_2$ and extends in-plane to both sides of them upon UVO exposing, as shown in the perspective view in the upper panel. Four different degree of oxidation regions revealed in Fig. 4 are displayed in the side view in the lower panel. Regions A are almost intact 3L MoS $_2$. The upper layer of regions B is 1D periodic parallel MoO $_x$ beneath which is two decoupled 1L MoS $_2$ with insertion of oxygen. The upper layer of regions C is discrete large clusters of MoO $_x$.

J. Liu et al. Results in Physics 19 (2020) 103634

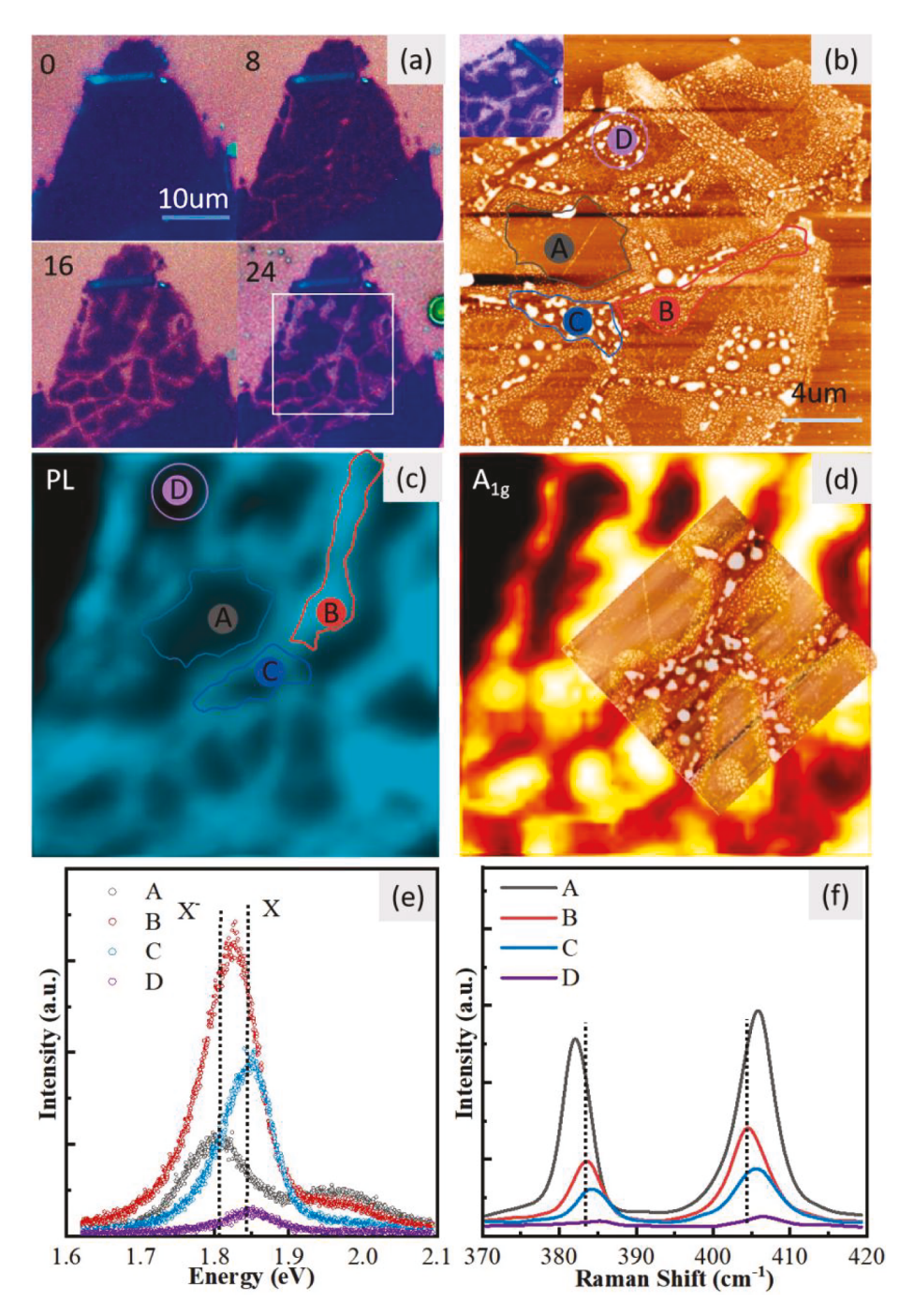


Fig. 4. 3L MoS_2 upon different treatment time. (a) Optical images of 3L MoS_2 with the representive 0, 8, 12 and 24 min treatment. (b) AFM image after 24 min treatment, the insert is the corresponding optical image. PL (c) and Raman A_{1g} peak (d) intensity images corresponding to the white solid square in (a). PL (e) and Raman (f) spectra extracted from locations #A, #B, #C and #D in (c).

Conclusion

In summary, we have systematically demonstrated the evolutions of morphology and electronic properties of the UVO treated exfoliated few-layered of MoS_2 . The XPS/UPS characterizations reveal a newly-formed MoO_x induced weak p-doping effect on account of charge transfer from MoS_2 to it. OM, AFM, Raman and PL mapping results demonstrate an inhomogeneous oxidation which is initiated at intrinsic defect sites and dislocations, and then expanded in-plane from dislocations to both sides to form one dimensional standing-wave-like features. However, the dangling-bond-free surface regions remain smooth due to the higher kinetic barrier for O_2 dissociation and chemisorption. A carton clearly

depicting the detailed inhomogeneous oxidation process has been proposed, which is rather different with the uniform one for $MoSe_2$ and $MoTe_2$ and can be attributed to the difference in the in-plane chemical bonds. Our findings can explain the worse effect of UVO exposure on the MoS_2 performance improvement. The inhomogeneous oxidation process in MoS_2 indicates the device design with UVO oxidation can not only take notice of the doping effect, but also need to take the microstructure changes after treatment into account.

CRediT authorship contribution statement

Jinxin Liu: Investigation, Writing - original draft, Writing - review &

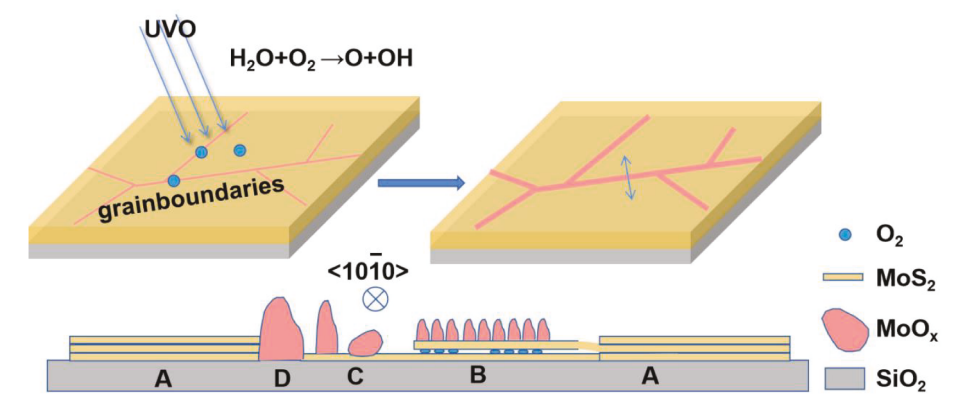


Fig. 5. Schematic diagram of the oxidation process of 3L MoS₂ exposed to UVO. (a) top view of the oxidation process which is initiated at grainboundaries and then expanded in-plane from grainboundaries to both sides. (b) side view of the oxidation process displays A, B, C and D regions.

editing. Kuanglv Sun: Data curation. Xiaoming Zheng: Data curation. Shitan Wang: Data curation. Shichang Lian: Data curation. Chuyun Deng: Resources. Haipeng Xie: Formal analysis. Xueao Zhang: Resources. Yongli Gao: Funding acquisition. Fei Song: Resources. Han Huang: Conceptualization, Methodology, Supervision, Funding acquisition.

Declaration of Competing Interest

The authors declare that they have no known competing financial interests or personal relationships that could have appeared to influence the work reported in this paper.

Acknowledgments

H. Huang acknowledges the support from the National Natural Science Foundation (NSF) of China (Grants No. 11874427). Y. Gao acknowledges the support from National Science Foundation DMR-1903962.

Appendix A. Supplementary data

Supplementary data to this article can be found online at https://doi.org/10.1016/j.rinp.2020.103634.

References

- [1] Novoselov KS, Geim AK, Morozov SV, Jiang D, Katsnelson MI, Grigorieva IV, et al. Two-dimensional gas of massless Dirac fermions in graphene. Nature 2005;438 (7065):197–200.
- [2] Samori P, Palermo V, Feng X. Chemical approaches to 2D materials. Adv Mater 2016;28(29):6027–9.
- [3] Fiori G, Bonaccorso F, Iannaccone G, Palacios T, Neumaier D, Seabaugh A, et al. Electronics based on two-dimensional materials. Nat Nanotechnol 2014;9(10): 768–79.
- [4] Geim AK, Van der Grigorieva IV. Waals heterostructures. Nature 2013;499(7459): 419–25.
- [5] Sun, L.; Chen, C.; Zhang, Q.; Sohrt, C.; Zhao, T.; Xu, G.; Wang, J.; Wang, D.; Rossnagel, K.; Gu, L.; Tao, C.; Jiao, L. Suppression of the Charge Density Wave State in Two-Dimensional 1T-TiSe(2) by Atmospheric Oxidation. Angewandte Chemie (International ed. in English) 2017, 56 (31), 8981-8985.
- [6] Castellanos-Gomez A, Vicarelli L, Prada E, Island JO, Narasimha-Acharya KL, Blanter SI, et al. V. Isolation and characterization of few-layer black phosphorus. 2d Materials 2014;1(2):025001.
- [7] Yu Y, Ma L, Cai P, Zhong R, Ye C, Shen J, et al. High-temperature superconductivity in monolayer Bi₂Sr₂CaCu2O_{8+delta}. Nature 2019;575(7781):156–63.
- [8] Shcherbakov D, Stepanov P, Weber D, Wang Y, Hu J, Zhu Y, et al. Raman spectroscopy, photocatalytic degradation, and stabilization of atomically thin chromium tri-iodide. Nano Lett 2018;18(7):4214–9.
- [9] Wood JD, Wells SA, Jariwala D, Chen KS, Cho E, Sangwan VK, et al. Effective passivation of exfoliated black phosphorus transistors against ambient degradation. Nano Lett 2014;14(12):6964–70.

- [10] Cui X, Lee GH, Kim YD, Arefe G, Huang PY, Lee CH, et al. Multi-terminal transport measurements of MoS2 using a van der Waals heterostructure device platform. Nat Nanotechnol 2015;10(6):534–40.
- [11] Li L, Engel M, Farmer DB, Han S, Wong HSP. High-performance p-type black phosphorus transistor with scandium contact. ACS Nano 2016;10(4):4672–7.
- [12] Kotsakidis JC, Zhang Q, Vazquez de Parga AL, Currie M, Helmerson K, Gaskill DK, et al. Oxidation of monolayer WS₂ in ambient is a photoinduced process. Nano Lett 2019;19(8):5205–15.
- [13] Zhang F, Zang Y, Huang D, Di C, Zhu D. Flexible and self-powered temperaturepressure dual-parameter sensors using microstructure-frame-supported organic thermoelectric materials. Nat Commun 2015;6(1):8356.
- [14] Mao D, Du B, Yang D, Zhang S, Wang Y, Zhang W, et al. Nonlinear saturable absorption of liquid-exfoliated molybdenum/tungsten ditelluride nanosheets. Small 2016;12(11):1489–97.
- [15] Vegamayoral V, Backes C, Hanlon D, Khan U, Gholamvand Z, Obrien M, et al. Photoluminescence from liquid-exfoliated WS2 monomers in poly(vinyl alcohol) polymer composites. Adv Funct Mater 2016;26(7):1028–39.
- [16] Ho PH, Chang YR, Chu YC, Li MK, Tsai CA, Wang WH, et al. High-Mobility InSe transistors: the role of surface oxides. ACS Nano 2017;11(7):7362–70.
- [17] Li Z, Yang S, Dhall R, Kosmowska E, Shi H, Chatzakis I, et al. Layer control of WSe2 via selective surface layer oxidation. ACS Nano 2016;10(7):6836–42.
- [18] Choudhary N, Islam MR, Kang N, Tetard L, Jung Y, Khondaker SI. Two-dimensional lateral heterojunction through bandgap engineering of MoS2 via oxygen plasma. J Phys Condens Matter 2016;28(36):364002.
- [19] Zheng X, Wei Y, Deng C, Huang H, Yu Y, Wang G, et al. Controlled layer-by-layer oxidation of MoTe₂ via O₃ exposure. ACS Appl Mater Interfaces 2018;10(36): 30045–50.
- [20] Zheng X, Wei Y, Liu J, Wang S, Shi J, Yang H, et al. A homogeneous p-n junction diode by selective doping of few layer MoSe₂ using ultraviolet ozone for highperformance photovoltaic devices. Nanoscale 2019;11(28):13469–76.
- [21] Zheng X, Zhang X, Wei Y, Liu J, Yang H, Zhang X, et al. Enormous enhancement in electrical performance of few-layered MoTe₂ due to Schottky barrier reduction induced by ultraviolet ozone treatment. Nano Res 2020;13(4):952–8.
- [22] Kang M, Yang HI, Choi W. Oxidation of WS₂ and WSe₂ monolayers by ultravioletozone treatment. J Phys D Appl Phys 2019;52(50):505105.
- [23] Chen F, Liu J, Zheng X, Liu L, Xie H, Song F, et al. Interfaces between MoOx and MoX2 (X=S, Se, and Te). Chin Phys B 2020.
- [24] Santosh KC, Longo RC, Wallace RM, Cho K. Surface oxidation energetics and kinetics on MoS2 monolayer. J Appl Phys 2015;117(13):135301.
- [25] Fang L, Yuan X, Liu K, Li L, Zhou P, Ma W, et al. Direct bilayer growth: a new growth principle for a novel WSe₂ homo-junction and bilayer WSe₂ growth. Nanoscale 2020;12(6):3715–22.
- [26] Wu D, Shi J, Zheng X, Liu J, Dou W, Gao Y, et al. CVD Grown MoS₂ nanoribbons on MoS₂ covered sapphire(0001) without catalysts. Phys Status Solidi (RRL) – Rapid Res Lett 2019;13(7):1900063.
- [27] He B, Tian G, Gou J, Liu B, Shen K, Tian Q, et al. Structural and electronic properties of atomically thin Bismuth on Au(111). Surf Sci 2019;679:147–53.
- [28] Jadwiszczak J, O'Callaghan C, Zhou Y, Fox DS, Weitz E, Keane D, et al. Oxide-mediated recovery of field-effect mobility in plasma-treated MoS₂. Sci Adv 2018;4 (3):eaao5031.
- [29] Azcatl A, McDonnell S, Santhosh KC, Peng X, Dong H, Qin X, Addou R, Mordi GI, Lu N, Kim J, Kim MJ, Cho K, Wallace RM. MoS₂ functionalization for ultra-thin atomic layer deposited dielectrics. Appl Phys Lett 2014;104(11):111601.
- [30] Baker MA, Gilmore R, Lenardi C, Gissler W. XPS investigation of preferential sputtering of S from MoS₂ and determination of MoS_x stoichiometry from Mo and S peak positions. Appl Surf Sci 1999;150(1-4):255-62.
- [31] Mak KF, Lee C, Hone J, Shan J, Heinz TF. Atomically thin MoS₂: a new direct-gap semiconductor. Phys Rev Lett 2010;105(13):136805.
- [32] Huang Y, Zhuge F, Hou J, Lv L, Luo P, Zhou N, et al. Waals coupled organic molecules with monolayer MoS₂ for fast response photodetectors with gate-tunable responsivity. ACS Nano 2018;12(4):4062–73.

- [33] Meyer J, Hamwi S, Kroger M, Kowalsky W, Riedl T, Kahn A. Transition metal oxides for organic electronics: energetics, device physics and applications. Adv Mater 2012;24(40):5408–27.
- [34] Peng, Liu, Xiaoliang, Liu, Lu, Lyu, Haipeng, Xie, Hong, Zhang. Interfacial electronic structure at the CH₃NH₃PbI₃/MoO_x interface. Appl Phys Lett 2015.
- [35] Zafar A, Nan H, Zafar Z, Wu Z, Jiang J, You Y, et al. Probing the intrinsic optical quality of CVD grown MoS₂. Nano Res 2016;10(5):1608–17.
- [36] Lee C, Yan H, Brus LE, Heinz TF, Hone J, Ryu S. Anomalous lattice vibrations of single- and few-layer MoS₂. ACS Nano 2010;4(5):2695–700.
- [37] Li SL, Miyazaki H, Song H, Kuramochi H, Nakaharai S, Tsukagoshi K. Quantitative Raman spectrum and reliable thickness identification for atomic layers on insulating substrates. ACS Nano 2012;6(8):7381–8.
- [38] Li H, Zhang Q, Yap CCR, Tay BK, Edwin THT, Olivier A, et al. From bulk to monolayer MoS₂: evolution of raman scattering. Adv Funct Mater 2012;22(7): 1385–90
- [39] Zhang X, Qiao XF, Shi W, Wu JB, Jiang DS, Tan PH. Phonon and Raman scattering of two-dimensional transition metal dichalcogenides from monolayer, multilayer to bulk material. Chem Soc Rev 2015;44(9):2757–85.
- [40] Splendiani A, Sun L, Zhang Y, Li T, Kim J, Chim CY, et al. Emerging photoluminescence in monolayer MoS₂. Nano Lett 2010;10(4):1271–5.
- [41] Yamamoto M, Einstein TL, Fuhrer MS, Cullen WG. Anisotropic etching of atomically thin MoS₂. J Phys Chem C 2013;117(48):25643–9.
- [42] Santosh KC, Longo RC, Wallace RM, Cho K. Surface oxidation energetics and kinetics on MoS2 monolayer. J Appl Phys 2015;117(13):135301.1–8.
- [43] Mirabelli G, Mcgeough C, Schmidt M, Mccarthy EK, Monaghan S, Povey IM, et al. Air sensitivity of MoS₂, MoSe₂, MoTe₂, HfS₂, and HfSe₂. J Appl Phys 2016;120(12): 125102
- [44] Liu H, Han N, Zhao J. Atomistic insight into the oxidation of monolayer transition metal dichalcogenides: from structures to electronic properties. RSC Adv 2015;5 (23):17572–81.

- [45] Lv D, Wang H, Zhu D, Lin J, Yin G, Lin F, et al. Atomic process of oxidative etching in monolayer molybdenum disulfide. Sci Bull 2017;62(12):846–51.
- [46] Wu D, Huang H, Zhu X, He Y, Xie Q, Chen X, et al. E" raman mode in thermal strain-fractured CVD-MoS₂. Crystals 2016;6(11):151.
- [47] Luo S, Hao G, Fan Y, Kou L, He C, Qi X, et al. Formation of ripples in atomically thin MoS₂ and local strain engineering of electrostatic properties. Nanotechnology 2015;26(10):105705.
- [48] Chen Q, Li H, Zhou S, Xu W, Chen J, Sawada H, et al. Ultralong 1D vacancy channels for rapid atomic migration during 2D void formation in monolayer MoS₂. ACS Nano 2018;12(8):7721–30.
- [49] Kang NR, Paudel HP, Leuenberger MN, Tetard L, Khondaker SI. Photoluminescence quenching in single-layer MoS₂ via oxygen plasma treatment. J Phys Chem C 2014; 118(36):21258–63.
- [50] Nan H, Wang Z, Wang W, Liang Z, Lu Y, Chen Q, et al. Strong photoluminescence enhancement of MoS₂ through defect engineering and oxygen bonding. ACS Nano 2014;8(6):5738-45.
- [51] Parkin WM, Balan A, Liang L, Das PM, Lamparski M, Naylor CH, et al. Raman shifts in electron-irradiated monolayer MoS₂. ACS Nano 2016;10(4):4134–42.
- [52] Dhall R, Neupane MR, Wickramaratne D, Mecklenburg M, Li Z, Moore C, et al. Direct bandgap transition in many-layer MoS₂ by plasma-induced layer decoupling. Adv Mater 2015;27(9):1573–8.
- [53] Yang A, Blancon J-C, Jiang W, Zhang H, Wong J, Yan E, et al. Giant enhancement of photoluminescence emission in WS₂-two-dimensional perovskite heterostructures. Nano Lett 2019;19(8):4852–60.
- [54] Ko TY, Jeong A, Kim W, Lee J, Kim Y, Lee JE, et al. On-stack two-dimensional conversion of MoS₂ into MoO₃. 2D Materials 2016;4(1):014003.
- [55] Mouri S, Miyauchi Y, Matsuda K. Tunable photoluminescence of monolayer MoS₂ via chemical doping. Nano Lett 2013;13(12):5944–8.